Influence of InGaN/GaN multiple quantum well structure on photovoltaic characteristics of solar cell

Noriyuki Watanabe[1*†], Manabu Mitsuhara[1†], Haruki Yokoyama[1†], Jianbo Liang[2], and Naoteru Shigekawa[2]

[1]NTT Photonics Laboratories, Nippon Telegraph and Telephone Corporation, Atsugi, Kanagawa 243-0198, Japan
[2]Graduate School of Engineering, Osaka City University, Osaka 588-8585, Japan
E-mail: watanabe.noriyuki@lab.ntt.co.jp

We have investigated InGaN/GaN multiple quantum well (MQW) solar cells in terms of the relationship between the short-circuit current and the MQW structure. We previously reported that higher short-circuit current is obtained in solar cells with thinner GaN barrier layers, and in this investigation, we also obtained higher short-circuit current in solar cells with higher numbers of InGaN/GaN periodic layers. These results can be explained by the hypothesis that the transport characteristics of photoinduced carriers are characterized by the specific length within which carriers photoinduced in the InGaN well layer can move before recombination. The carrier collection efficiency is improved by the drift in the barrier layer due to the forward internal electric field and degraded by the carrier accumulation in the well layer caused by the inverse internal electric field and the potential barrier between layers, which well describes the influence of the MQW structure on the specific length. Using this model, we discuss how we can determine the MQW structure that yields higher short-circuit current, and conclude that the optimum thickness of the InGaN well layer is about 2–3 nm when the thickness of the GaN barrier layer is 3–8 nm. © 2014 The Japan Society of Applied Physics

1. Introduction

Photovoltaic energy conversion is one of the promising technologies for generating renewable, carbon-free electric power. The amount of solar energy that the earth receives from the sun each day is huge and is considered to exceed the amount of energy consumed in the world. However, the solar energy density ($100\,\mathrm{mW\cdot cm^{-2}}$) is low and the conversion efficiency of solar cells is insufficient, so that very expansive areas of solar cells would be necessary to meet the world's energy needs. One of the solutions is to develop high-conversion-efficiency solar cells. The use of multijunction tandem solar cells, which have several subcells composed of a different band-gap material, is the most effective way to achieve high conversion efficiency. The use of several subcells with different band gaps could increase the total usable solar energy.

Group-III nitrides are attractive semiconductors for fabricating solar cells with high conversion efficiency. This is because the band gap of a ternary or quaternary compound can be controlled to any value between 0.65 eV (for InN) and 6.2 eV (for AlN) simply by changing the composition.[1–3] In particular, InGaN is attracting much interest because its band-gap energy range (0.65–3.4 eV) covers most of the solar spectrum, which is advantageous for the effective use of solar energy. This means that the current-matching condition, which is required for high conversion efficiency, can be easily achieved by using the InGaN system. For example, Yamamoto et al. predicted that the conversion efficiency of a multijunction tandem cell with over six junctions should exceed 50% even under the condition of 1 sun.[4] In this decade, many investigations of InGaN-based solar cells have been reported.[5–36] However, the cell performance is still not nearly as high as expected. This is because of the difficulty growing an InGaN layer with a suitable band-gap energy and a sufficient crystal quality for achieving good photovoltaic performance. Therefore, many recent investigations have focused on improving the InGaN quality. For example,

Kuwahara et al. reported that using a GaN substrate[25] and a multiple quantum well (MQW) structure[26] for InGaN-based solar cells is effective for improving the photovoltaic characteristics.

As the use of MQW is very effective for improving the conversion efficiency of InGaN-based solar cells, several investigations have focused on the influence of the MQW structure on photovoltaic behaviors. For example, Wierer et al. investigated the influence of barrier thickness and reported that a thinner GaN barrier layer resulted in higher short-circuit current.[32] A similar tendency was observed in our previous work.[37] In that work, we speculated that the transport and radiative recombination processes of photo-induced carriers might affect the short-circuit current. The photovoltaic behaviors of InGaN/GaN MQW solar cells with various numbers of wells were investigated by Farrell et al.[30] and Valdueza-Felip et al.,[34] and both reported that increasing the number of wells increased the short-circuit current. However, they did not give any reasons for this behavior. In this study, we examine the relationship between the MQW structure and the photovoltaic properties, focusing especially on the short-circuit current of InGaN/GaN MQW solar cells. First, we propose a simple model for estimating the short-circuit current of InGaN/GaN MQW solar cells. This model is represented by a specific length within which carriers photoinduced in the InGaN well layer can move before recombination. The validity of this model is confirmed from experimental results. Subsequently, we examine the suitable structure of the InGaN/GaN MQW for achieving high short-circuit current.

2. Experimental procedure

Solar cell structures were grown by the low-pressure metal-organic chemical vapor deposition method on 2-in.-diameter n-type GaN free-standing substrates. The threading dislocation density of the GaN substrate was less than $10^8\,\mathrm{cm^{-2}}$. The group-III sources were trimethylgallium for n-type GaN growth, and triethylgallium and trimethylindium for MQW and p-contact layer growth. The nitrogen source was ammonia. Silane was used for n-type doping and Cp_2Mg was used for p-type doping.

†Present address: NTT Device Technology Laboratories, Nippon Telegraph and Telephone Corporation, Atsugi, Kanagawa 243-0198, Japan.
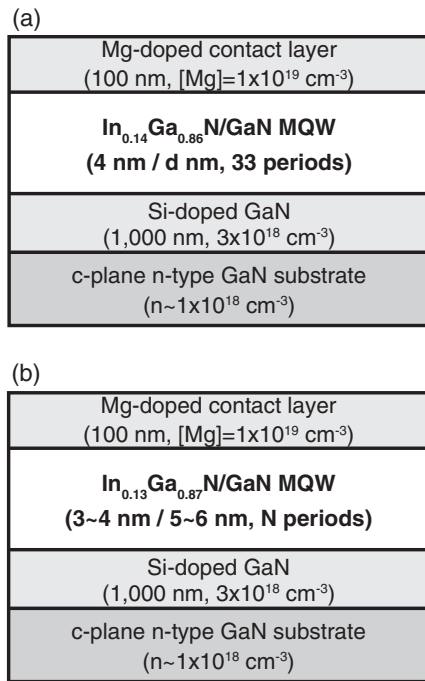
Fig. 1. Epitaxial layer structures of solar cells with InGaN/GaN MQW absorption layers. (a) Series A: different barrier thicknesses (3 and 9 nm), the same well thickness, and the same number of InGaN well layers. (b) Series B: different numbers of wells (5, 10, and 20 pairs) and the same InGaN/GaN unit QW layers.

Fig. 2. (Color online) J–V curves of InGaN/GaN MQW solar cells under AM 1.5 G illumination.

The epitaxial layer structures of solar cells are shown in Fig. 1. We prepared two series of MQW structures (series A and series B). Two samples in series A have MQW structures with different barrier thicknesses: the thickness of the GaN barrier layer is 3 nm (sample A-1) or 9 nm (sample A-2) and the well layer of $In_{0.13}Ga_{0.87}N$ in both has the same thickness (4 nm). The MQWs of both samples have the same number of InGaN/GaN periodic layers, 33. These samples in series A are the same as those used in our previous work.[37] Series B comprises three samples that have the same InGaN/ GaN period: 5–6-nm-thick GaN barrier and 3–4-nm-thick $In_{0.14}Ga_{0.86}N$ well layer. The numbers of InGaN/GaN periodic layers in the three samples are 5 (sample B-1), 10 (sample B-2), and 20 (sample B-3). We determined the MQW structure parameters using high-resolution X-ray diffraction (HR-XRD). By reciprocal space mapping of HR-XRD, we confirmed that each epitaxial layer was coherently grown on the GaN substrate. To evaluate the dislocation density in the MQW, we took cross-sectional transmission electron microscope images for series A, which has the maximum number of InGaN/GaN periodic layers in this investigation. No dislocations were observed in the MQWs of samples A-1 and A-2. Therefore, we believe that the dislocation density in the MQWs is almost the same as that in the GaN substrate (less than 10^8 cm^{-2}).

Solar cells with dimensions of 2×2 mm^2 for series A or 5×5 mm^2 for series B were fabricated over the entire 2-in. wafer. The n-contact metal of Ti/Al/Ni/Au was evaporated to the back of the wafer, and the p-contact grid metal of Ni/Au was formed by evaporation and the lift-off method. There is no current spreading layer. Before forming the p-contact grid metal, the wafers were annealed at 850 °C
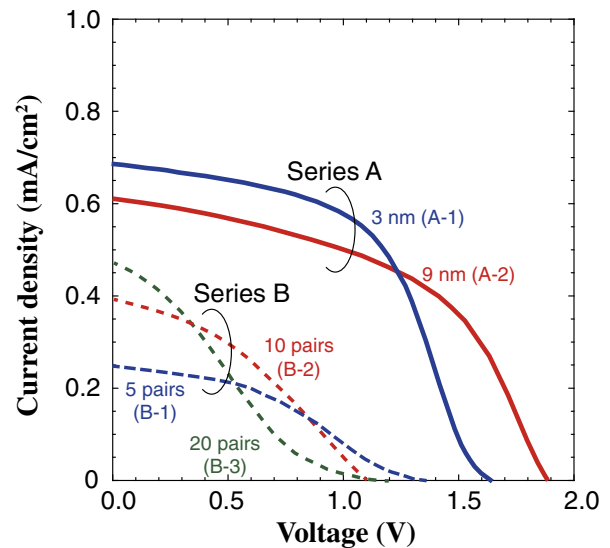
for 10 min in a N$_2$ ambient to activate Mg acceptors. The top surface of each cell was coated with an antireflection layer. The devices were isolated from each other by inductively coupled plasma etching. We tested for photovoltaic characteristics of the fabricated solar cells. The current–voltage characteristics were measured under air-mass 1.5 global (AM1.5G) illumination (power density of 100 mW/cm^2) produced by a solar simulator.

The lifetime of photo-induced carriers of solar cell structures was evaluated using time-resolved photoluminescence (TRPL) spectra measured at room temperature. The excitation source was a laser diode with an incident wavelength of 375 nm. For comparison, we also measured TRPL of several samples with various MQW structures grown on sapphire substrates. The photoluminescence (PL) spectra of solar cell structures on GaN substrates and MQW structures on sapphire substrates were also measured at room temperature. The excitation source was a He–Cd laser with an incident wavelength of 325 nm.

3. Results

3.1 Photovoltaic performance

Although the photovoltaic characteristics of samples A-1 and A-2 have already been reported,[37] we again summarize them in this section for the readers' convenience. Current–voltage characteristics under illumination are plotted in Fig. 2. The solar cell parameters evaluated from the data in Fig. 2 are summarized in Table I. For series A, with a thinner barrier layer, the short-circuit current density J_{SC} increases and the open-circuit voltage V_{OC} decreases. The fill factor (FF) of both solar cells is approximately 50%, resulting in a similar maximum output power, that is, a similar conversion efficiency η. For series B, with an increase in the number of InGaN/GaN periodic layers in the MQW structure (N), the value of J_{SC} increases. The value of V_{OC} seems to be independent of the value of N. Small values of FF of about 20–40% result in very small η of about 0.12–0.15%. This is because all series-B samples show very high series resistance and relatively low shunt resistance.

Table I.   Parameters of InGaN/GaN MQW solar cells.

	Series A		Series B		
	A-1	A-2	B-1	B-2	B-3
J_{SC} (mA/cm^2)	0.69	0.61	0.25	0.39	0.47
V_{OC} (V)	1.64	1.89	1.35	1.11	1.20
FF (%)	53	49	38	36	22
η (%)	0.60	0.57	0.13	0.16	0.12
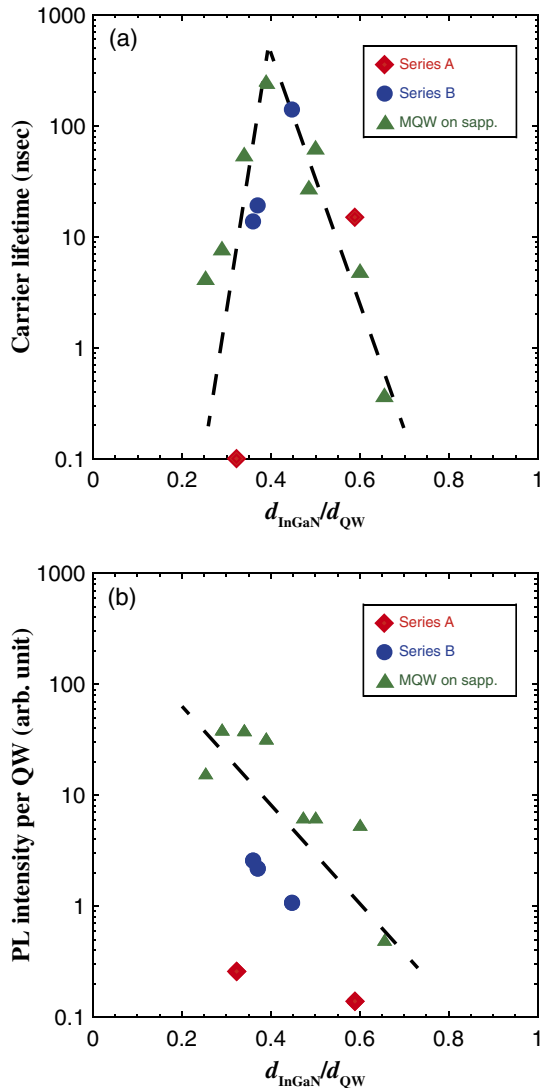
Fig. 3.   (Color online) MQW structure dependence of (a) the lifetime of photoinduced carriers estimated from TRPL and (b) the PL intensity per QW. Broken lines are guides for the eyes.

3.2   Influence of MQW structure on carrier lifetime

In general, the value of J_{SC} correlates with the lifetime of photoinduced carriers. The carrier lifetime τ can be estimated from TRPL spectra. Figure 3(a) shows the dependence of τ on the MQW structure, and Fig. 3(b) shows a plot of the dependence of the PL intensity per QW. In Fig. 3, we also plot measured values for several MQW structures with various well and barrier layer thicknesses grown on sapphire substrates. The value of τ strongly depends on the ratio between the thickness of the InGaN (d_{InGaN}) well layer and that of one QW period (d_{QW}). In the region in which the ratio

between d_{InGaN} and d_{QW} is smaller than 0.4, τ also rapidly increases as the ratio increases. As the ratio further increases, τ suddenly decreases. In contract, the PL intensity monotonically decreases as the ratio between d_{InGaN} and d_{QW} increases; the intensity itself is different between the sample series.

This dependence of the lifetime on the MQW structure can be explained as follows. The carrier lifetime τ is determined by two components. One is the carrier lifetime specified by radiative recombination (indicated as τ_R). The other is the carrier lifetime governed by nonradiative recombination (indicated as τ_{NR}). The value of τ is given as $\tau^{-1} = \tau_R^{-1} + \tau_{NR}^{-1}$, and increasing the InGaN thickness might affect both τ_R and τ_{NR}. Because of the strong polarization effect, an internal electric field is formed in the band profile of the InGaN/GaN MQW and the photoinduced electrons and holes are spatially separated from each other (the quantum confined Stark effect). Figure 4 shows the calculated band profiles and electronic states (wave functions).[38] When the InGaN layer thickness is small, the separation between electrons and holes is relatively small and radiative recombination occurs between the photoinduced carriers in the same well layer [Fig. 4(a)]. In this case, the radiative recombination rate should be very large, resulting in a very short carrier lifetime. As the InGaN thickness increases, the separation between photoinduced electrons and holes increases. In this situation, the radiative recombination process could occur between electrons and holes both in the same InGaN well layer and in the next InGaN well layer [Fig. 4(b)], and the recombination rate should become small, resulting in larger τ_R. In contrast, the InGaN thickness would have an inverse effect on the nonradiative recombination process. As shown in Fig. 3(b), the PL intensity per QW decreases as the InGaN thickness increases. This tendency could be roughly considered to be due to the enhancement of the nonradiative recombination with increasing InGaN thickness. In other words, τ_{NR} decreases as the InGaN thickness increases. The effects of increasing the InGaN thickness on both the radiative and nonradiative recombinations would cause the carrier lifetime dependence on the InGaN thickness shown in Fig. 3(a).

3.3   Influence of MQW properties on short-circuit current

Figure 5 shows the dependence of J_{SC} on the carrier lifetime τ, estimated from TRPL spectra. The values of J_{SC} in both series A and series B show a small dependence on the lifetime. These results suggest that the recombination process does not dominate J_{SC}.

Incidentally, the value of J_{SC} should be correlated with the number of photons absorbed in the MQW. More photons could be absorbed as the number of wells (N) is increased, resulting in larger J_{SC}. Figure 6 indicates how J_{SC} increases with increasing N. The solid line is a guide for the eyes. The value of J_{SC} is well fitted with the same line for both series and shows a linear dependence on the square root of N. If all the photoinduced carriers produced by photon absorption could reach the contact layer, the value of J_{SC} should show an approximately linear dependence on N. However, as shown in Fig. 6, the actual J_{SC} shows a weaker dependence on N than expected. These results suggest that the recombination process affects the carrier collection process of the MQW solar cells in both series A and series B. Therefore, we can consider that the recombination process of the photoinduced
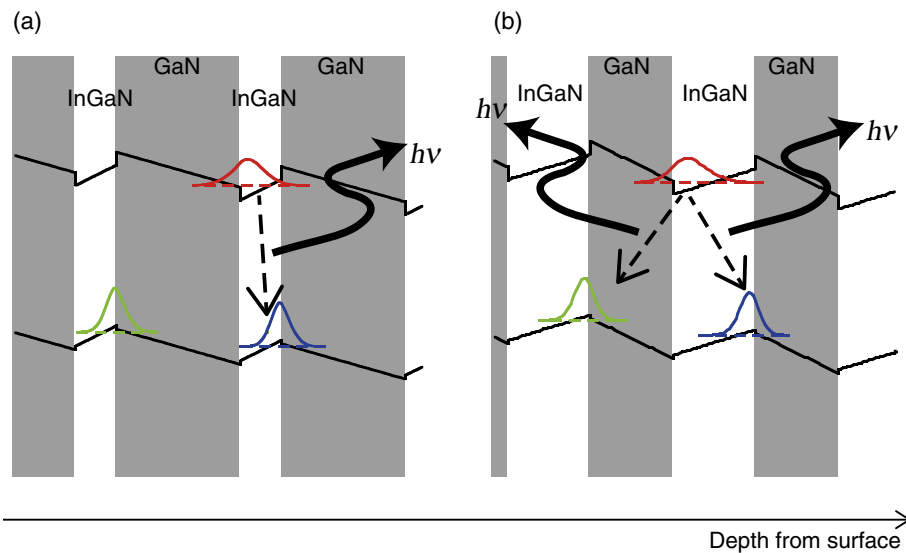
Fig. 4. (Color online) Schematic band profiles of the InGaN/GaN MQWs with different barrier and well layer thicknesses and wave functions of electrons in the conduction band and holes in the valence band: (a) $d_{InGaN} < d_{GaN}$ and (b) $d_{InGaN} \approx d_{GaN}$.
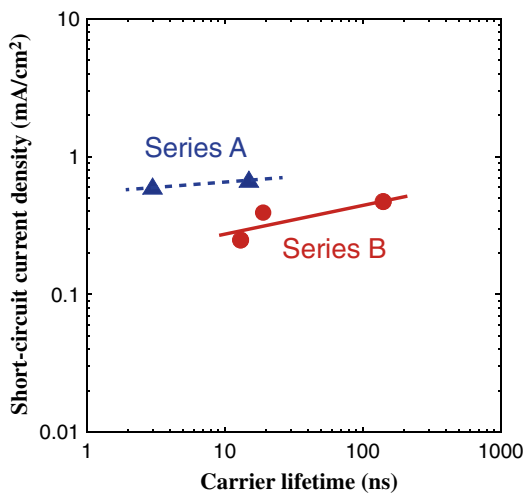
Fig. 5. (Color online) Carrier lifetime dependence of short-circuit current density.
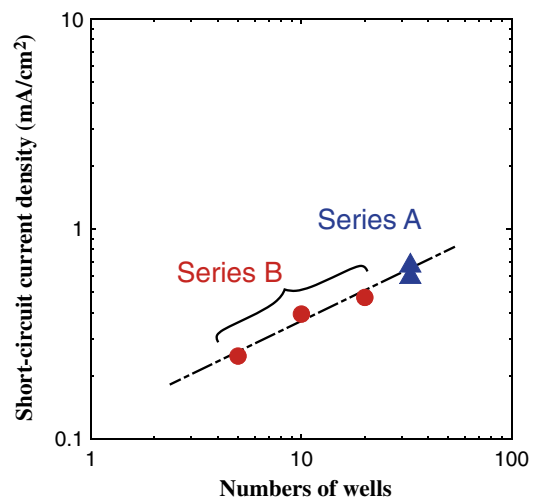
Fig. 6. (Color online) Dependence of short-circuit current density on the number of wells in InGaN/GaN MQW.

carriers should be taken into account, although the short-circuit current is mainly limited by the number of photons absorbed in the MQW layer.

4. Discussion

4.1 Simple model for estimating J_{SC}

In this section, we propose a simple model that enables the numerical estimation of J_{SC} of MQW solar cells. The following assumptions are made in the model.

(a) Photons in solar light penetrating into solar cells are only absorbed in InGaN well layers, not in GaN barrier layers.

(b) Photons with energy lower than the band-gap energy of the InGaN well layer pass completely through the well and barrier layers, and those with the same energy as or higher energy than the band-gap energy of the InGaN well layer are absorbed with the absorption coefficient α, and carriers (electrons and holes) are induced in the InGaN well layer.

(c) A fraction of photoinduced carriers in an InGaN well layer can reach contact layers; that is observed as short-circuit current. The transport process of photoinduced carriers can be represented by a specific length L. The specific length L is defined such that the existence probability of photoinduced carriers after moving the distance L is $1/e$, where e is the natural logarithm base.

(d) The specific lengths for electrons and holes are considered to be the same.

In assumption (c), we define the specific length L. This corresponds to the diffusion length when the carrier transport is mainly governed by a diffusion process. However, the absorption region of the solar cells used in this investigation is the MQW structure, and the internal electric field due to the strong polarization effect exists in both the InGaN well layer and the GaN barrier layer (Fig. 7). In this situation, the carrier transport should be governed not by a simple diffusion process, but by a complex effect of several processes such as drift, diffusion, and tunneling. Therefore, we consider
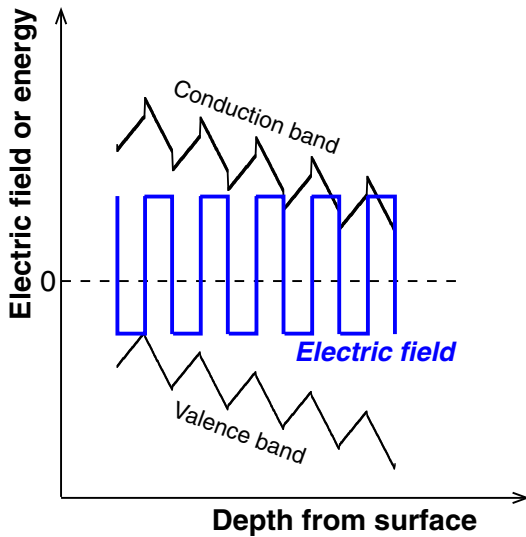
Fig. 7. (Color online) Schematic plots of band profiles and internal electric field for MQW structure.

Fig. 8. (Color online) Short-circuit current density of series-B samples as a function of the number of well layers in InGaN/GaN MQW. Curves show results calculated using Eq. (4) with various specific lengths.

the specific length L to be like a diffusion length in such a complex carrier transport in which several processes might be intricately entangled.

First, we investigate the photon absorption process in the InGaN well layer. According to assumptions (a) and (b), the intensity of solar radiation after the radiation has passed through the n-th InGaN well layer from the surface is given by

$$I_n = I_0 \exp(-n\alpha w_W), \qquad (1)$$

where I_0 and I_n are the initial intensity of solar radiation and that of the radiation after passing through the n-th InGaN well layer, respectively, and w_W is the thickness of the InGaN well layer. Next, we consider the transport process of photo-induced carriers from the MQW to contact layers. Most of the photoinduced carriers disappear during the radiative recombination process (i.e., PL) or nonradiative recombination process at some dislocations or defects, and only a fraction of photoinduced carriers can reach the contact layer to be detected as photocurrent. As shown in Fig. 1, the p-contact layer is on the surface of the cell and the n-contact is on the back of the wafer. Therefore, photoinduced holes rise to the surface of the cell and electrons descend to the back of the wafer and are detected as photocurrent. Holes photoinduced in the n-th InGaN well layer from the surface must move a distance $n(w_B + w_W)$ and electrons must move a distance $(N - n)(w_B + w_W)$. Here, w_B is the thickness of the GaN barrier layer. According to assumption (c), the probabilities of holes and electrons photoinduced in the n-th well layer reaching the p- and n-contact layers, respectively, are given by

$$\eta_p(n) = \exp\left[-\frac{n(w_B + w_W)}{L_p}\right], \qquad (2)$$

$$\eta_n(n) = \exp\left[-\frac{(N - n + 1)(w_B + w_W)}{L_n}\right], \qquad (3)$$

where L_p and L_n are the specific lengths for holes and electrons, and the values of L_p and L_n are the same according to assumption (d). Using Eqs. (1)–(3), we can express the short-circuit current density as
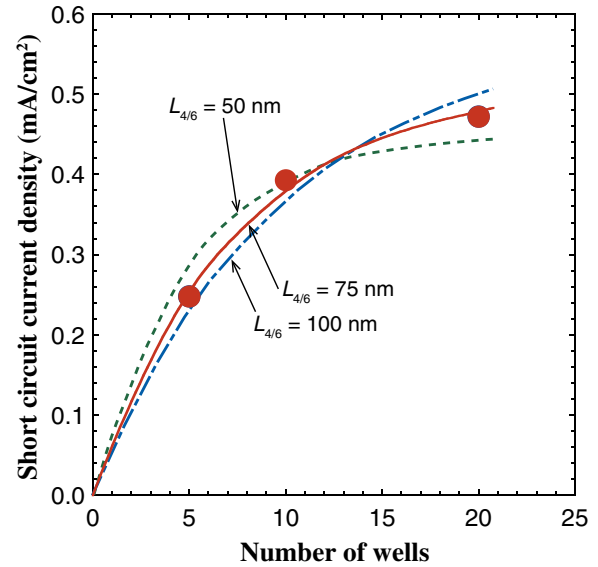
$$J_{SC} = A \sum_{n=1}^{N} (I_{n-1} - I_n)[\eta_n(n) + \eta_p(n)], \qquad (4)$$

where A is a fitting parameter.

4.2 Comparison with experimental data

In this section, we will compare the model introduced in the previous section with experimental results to verify of the model. Figure 8 shows the J_{SC} dependence of the number of wells on a linear scale for series B. In Fig. 8, three curves indicate the calculated results for various specific lengths using Eq. (4). Here, we used the value of $1 \times 10^5 \, \text{cm}^{-2}$ as α,[1] and the specific length was constant for all series-B samples. The values of the specific length ($L_{4/6}$) used in the calculation were 50, 75, and 100 nm. A larger specific length means that the photoinduced carriers in the well far from the contact layer can easily reach the contact layer and be detected as current. In this case, the curve of the dependence of J_{SC} on the number of well layers approaches a straight line. On the other hand, when the specific length is small, only the photoinduced carriers generated in the well layer near the contact layer can be detected as a current, resulting in the weak dependence of J_{SC} on the number of well layers. As shown in Fig. 8, experimental results agree best with the curve calculated for the specific length of 75 nm. Therefore, we can conclude that the value of $L_{4/6}$ is 75 nm.

Here, we will attempt to apply our model to previous data from other research groups.[30,34] Figure 9 shows the J_{SC} dependence of the number of wells on a linear scale for the results in Refs. 30 and 34. Blue and green curves indicate the results of calculation using Eq. (4) for data from each report, as for our series-B samples. The specific lengths are estimated to be 500 nm for Ref. 30 and 2,200 nm for Ref. 34 (expressed as $L_{\text{Ref.30}}$ and $L_{\text{Ref.34}}$, respectively). Both results are also well fitted with the calculated curves, similar to our results. These findings suggest that the model with assumptions (a)–(d) is appropriate for simulating the short-
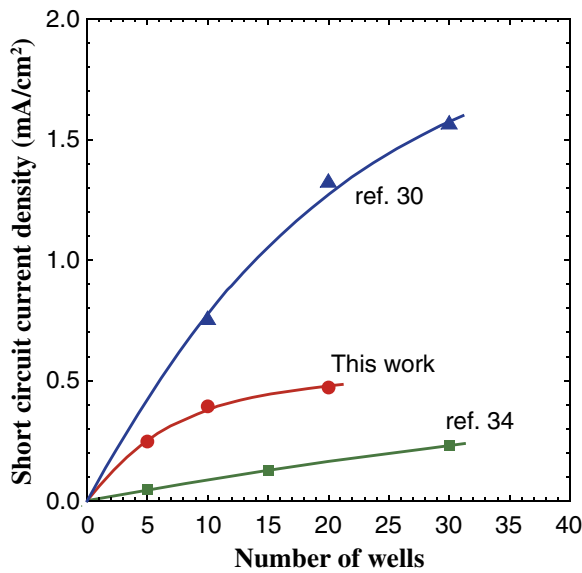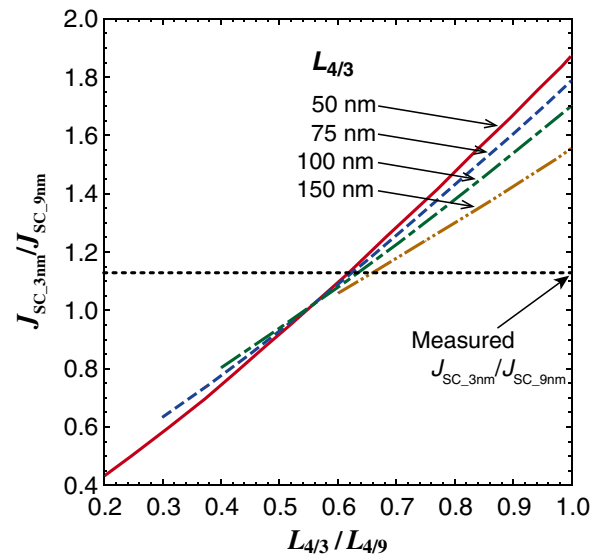
Fig. 9. (Color online) Dependence of short-circuit current density on the number of wells in InGaN/GaN MQW for samples in our series B, Refs. 30 and 34.

Fig. 10. (Color online) Specific length of the MQW solar cells from this work, Ref. 30, and Ref. 34 as a function of the ratio of InGaN well thickness to the GaN barrier thickness.

circuit current of InGaN/GaN MQW solar cells, and the specific lengths of photoinduced carriers of samples in Refs. 30 and 34 should be about 500 and 2,200 nm, respectively.

As discussed above, our proposal model could be considered to be adequate for estimating the short-circuit current. Hence, we will extend the model based on Eq. (4) to series-A samples; that is, we will discuss the influence of the barrier thickness on short-circuit current. As shown in Fig. 1, the difference between series-A and series-B samples is not only the number of InGaN wells but also the thickness of the GaN barrier layer. The difference in the barrier thickness should affect the specific length, resulting in a different value of L. In series A, both samples have the same number of wells. Therefore, we could not estimate their specific lengths as we did for series-B samples. Then, we attempted to estimate the ratio between $L_{4/3}$ and $L_{4/9}$ as follows. First, we calculated J_{SC} for sample A-1 (J_{SC_3nm}) and sample A-2 (J_{SC_9nm}) using Eq. (4) with certain values of $L_{4/3}$ and $L_{4/9}$ and plotted the ratio of the calculated J_{SC_3nm} to J_{SC_9nm} against the ratio of $L_{4/3}$ to $L_{4/9}$. Then, we obtained the actual value of L_{3nm}/L_{9nm} by comparing the calculated J_{SC_3nm}/J_{SC_9nm} with the experimental values of J_{SC_3nm}/J_{SC_9nm} listed in Table I. Figure 10 shows the dependence of the calculated J_{SC_3nm}/J_{SC_9nm} on $L_{4/3}/L_{4/9}$ for various $L_{4/3}$ values. In Fig. 10, the value of J_{SC_3nm}/J_{SC_9nm} from the experimental data is shown by a dotted line. Although the behavior of the calculated values of J_{SC_3nm}/J_{SC_9nm} against $L_{4/3}/L_{4/9}$ shows a slight difference with a change in $L_{4/3}$, they agree well when the value of $L_{4/3}/L_{4/9}$ is about 0.6–0.65. From this result, we could hypothesize that the specific length has a roughly linear dependence on the square root of the barrier thickness. Since we have already estimated $L_{4/6}$ to be 75 nm, we can estimate $L_{4/3}$ and $L_{4/9}$ to be 55 and 90 nm, respectively.

4.3　Influence of MQW structure on specific length
In this section, we will discuss the relationship between the specific length estimated in the previous section and the MQW structure. In general, the short-circuit current is mainly determined by two factors: the number of absorbed photons and the carrier collection efficiency. The latter is strongly affected by the recombination process of photo-induced carriers (specified by carrier lifetime) and the transport properties, such as the diffusion process (specified by diffusion length and mobility) or the drift process. These processes are thought to be complicatedly related to each other. Therefore, to simplify the discussion, the specific length is defined as a parameter that specifies the overall carrier collection process. As shown in the previous section, the value of the specific length changes in accordance with the MQW structure (i.e., the thickness of the InGaN well layer or GaN barrier layer). Figure 11 shows the specific length dependence of the ratio of the thickness of the InGaN well layer (w_W) to that of the GaN barrier layer (w_B). The value of the specific length decreases as the value of w_W/w_B increases. When w_B varies while w_W is constant, the specific length shows a relatively weak dependence on w_W/w_B. On the other hand, when the value of w_W decreases from 4 to 1.3 nm under constant w_B, the specific length rapidly increases from less than 100 nm to over 2 μm. The value of L is almost linear to $(w_W)^{-3}$. Therefore, we can conclude that the specific length (that is, the carrier collection efficiency) is strongly affected by the thickness of the InGaN well layer.

This behavior can be explained by the difference in the role of carrier transport between the InGaN well and the GaN barrier. As mentioned in Sect. 4.1, there are internal electric fields in the MQW region owing to the strong polarization effect of nitride semiconductors (Fig. 12). As shown in Fig. 12, the electric field in GaN barrier layers enhances the carrier transport by means of a drift process. Therefore, the GaN barrier layer should make the specific length longer. On the other hand, InGaN well layers inversely interfere with the carrier transport, because the direction of the electric field in the InGaN layer is the opposite of that in the GaN barrier layer and a large potential barrier exists at the interface
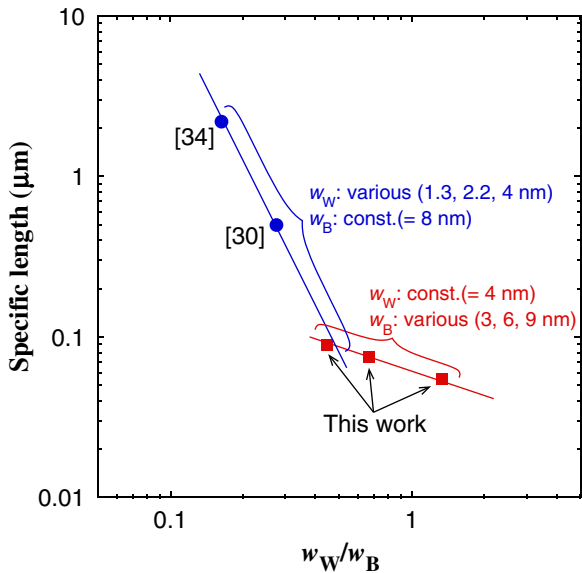
Fig. 11. (Color online) Calculated short-circuit current vs number of InGaN wells with various barrier thicknesses. The specific length also changes with changing barrier thickness.
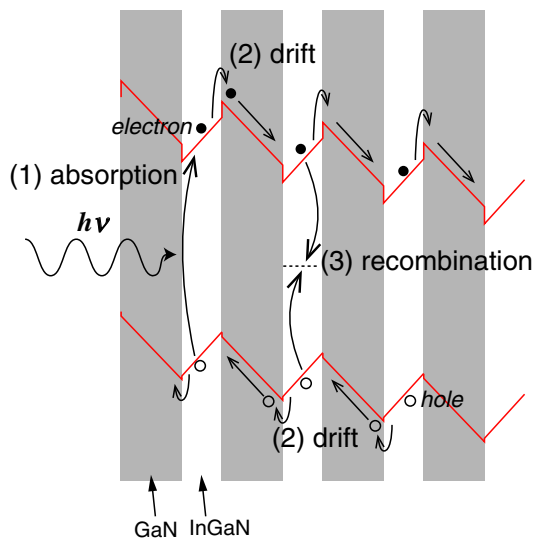
Fig. 12. (Color online) Schematic plots of band profiles and the elementary process of the solar cell operation in the MQW structure: (a) photon absorption in the well layer, (b) transport of the photoinduced carrier in the barrier layer (drift), and (c) carrier disappearance through nonradiative recombination process.

between the layers, resulting in the accumulation of the carriers in the InGaN well layer. Additionally, the influence of the recombination process must be taken into account. The carriers accumulated in the InGaN well layer should easily disappear through the radiative and nonradiative recombination processes. Both effects of the InGaN well layer might make the specific length smaller. On the basis of these ideas, the behavior shown in Fig. 11 can be explained as follows. For our samples, the thickness of the InGaN well layer (= 4 nm) is relatively large. Therefore, the effect of the InGaN layer, by which the specific length decreases, might be dominant compared with the effect of the GaN barrier layer. In particular, the influence of the recombination process
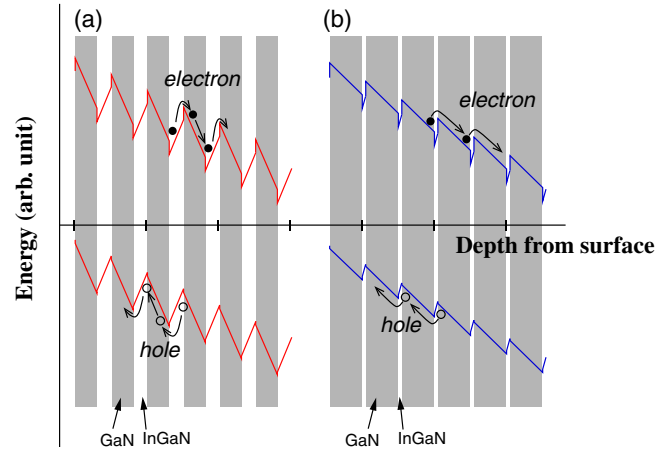

Fig. 13. (Color online) Schematic plots of band profiles of MQW with (a) $w_B \approx w_W$ and (b) $w_W \ll w_B$.

could be considerable. These behaviors would explain why the specific length is comparatively small and shows a brelatively weak dependence on the barrier thickness. In contrast, the samples used in Refs. 30 and 34 had a thinner InGaN well layer than ours, and the GaN barrier (= 8 nm) is much thicker than the InGaN well (= 1–2 nm). In this situation, the drift effect due to the GaN barrier layer should become much stronger and the potential barrier at the interface between InGaN and GaN seemingly becomes small (as shown in Fig. 13). As a result, the carrier transport might be mainly dominated by the drift process in the GaN barrier, resulting in the large specific length.

4.4 Influence of MQW structure on short-circuit current

As mentioned above, the specific length (in other words, the carrier collection efficiency) can be improved with a thin InGaN well layer and a thick GaN barrier layer. However, these changes in the MQW structure would cause the number of photons absorbed in the MQW to vary, resulting in a change in the short-circuit current. In this section, we will discuss the optimum MQW structure for improving the short-circuit current by taking the variation in the absorption edge energy of the MQW into account.

First, we calculated the maximum short-circuit current (J_{SC_max}) for the MQW with various InGaN well layer thicknesses. The fitting parameter A in Eq. (4) should include the number of photons absorbed in the MQW as a factor, and we assumed that it was proportional to the number of photons in the solar spectrum of AM1.5G,[39] whose energy is higher than the absorption edge energy of the MQW. Here, the In content in the InGaN well layer is 0.15 or 0.28. Because the barrier thickness negligibly affects the absorption edge energy, as shown in our previous report,[37] the thickness of the GaN barrier layer was set constant at 8 nm. The value of the absorption edge energy was calculated using the NEXTNANO3 software package.[38] Figure 14 shows how the J_{SC_max} calculated using Eq. (4) depends on the thickness of the InGaN well layer. The value of J_{SC_max} gradually increases as the InGaN well layer thickness decreases regardless of the In content in InGaN well layers. This is because the specific length increases with thinning of the well layer. At the InGaN layer thickness of 1 nm for the
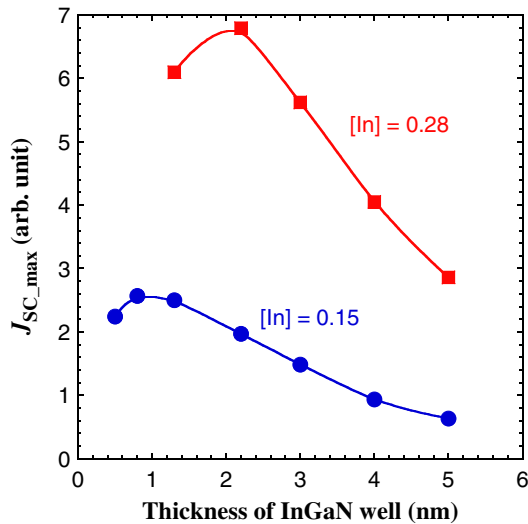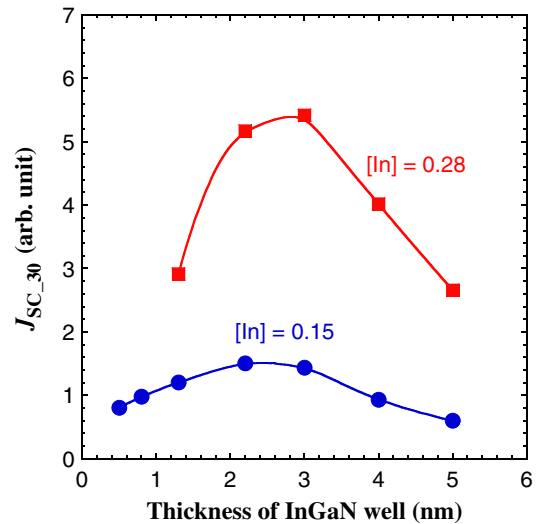
Fig. 14. (Color online) Calculated maximum short-circuit current of InGaN/GaN MQW solar cell as a function of the thickness of the InGaN well layer.

Fig. 15. (Color online) Calculated short-circuit current of 30-period-MQW solar cell as a function of the thickness of the InGaN well layer.

In content of 0.15 and 2 nm for 0.28 In, the value of J_{SC_max} becomes maximum. As the thickness of the InGaN well further decreases, J_{SC_max} also decreases. The reduction in J_{SC_max} is probably due to the decreasing number of absorbable photons as a result of the absorption edge energy decrease.

As shown in Fig. 14, the optimum thickness of the InGaN well layer could be considered to be about 1 nm. However, with such a thin well layer, a huge number of InGaN/GaN periodic layers is necessary for obtaining J_{SC_max}. For example, the J_{SC_max} value for the 1 nm MQW is obtained with over 200 periodic layers. This would result in difficulty in growing the samples. Therefore, we attempt to estimate the optimum well thickness in the situation where the number of InGaN/GaN periodic layers is not very large (typically, less than 50). The value of J_{SC} of the 30-period-MQW structure (J_{SC_30}) versus the thickness of the InGaN well layer is shown in Fig. 15 as an example. Regardless of the In content, the maximum value of J_{SC_30} is obtained at the InGaN well layer thickness of about 2–3 nm. At this thickness, the value of J_{SC_30} is considered to be almost the same as the value of J_{SC_max}. These findings suggest that the optimum thickness of the InGaN well layer for obtaining good short-circuit current while ensuring the ease of sample growth is 2–3 nm.

5. Conclusions

In this study, we investigated how the InGaN/GaN MQW structure affects the photoinduced carrier properties and photovoltaic behaviors, especially the short-circuit current. It was found that the radiative carrier lifetime has little influence on the short-circuit current, although it strongly depends on the MQW structure. It was also found that the short-circuit current is governed by the transport properties of photoinduced carriers characterized by the specific length within which carriers photo-induced in the InGaN well layer can move before recombination. We proposed a model based on several simple assumptions. This model can successfully describe the behavior of the short-circuit current with various

MQW structures of not only our samples but also those of other research groups. The difference in specific length between these samples can be well explained to be a result of the combination of the carrier drift in the GaN barrier layer and the carrier accumulation in the InGaN well layer. On the basis of the model and taking the number of absorbable photons into account, we can conclude that the optimum thickness of the InGaN well layer is about 2–3 nm when the thickness of the GaN barrier layer is 3–8 nm.

1) J. Wu, W. Walukiewicz, K. M. Yu, J. W. Ager, III, E. E. Haller, H. Lu, and W. J. Schaffs, Appl. Phys. Lett. **80**, 4741 (2002).
2) W. Walukiewicz, S. X. Li, J. Wu, K. M. Yu, J. W. Ager, III, E. E. Haller, H. Lu, and W. J. Schaff, J. Cryst. Growth **269**, 119 (2004).
3) R. E. Jones, R. Broesler, K. M. Yu, J. W. Ager, III, E. E. Haller, W. Walukiewicz, X. Chen, and W. J. Schaff, J. Appl. Phys. **104**, 123501 (2008).
4) A. Yamamoto, Md. R. Islam, T.-T. Kang, and A. Hashimoto, Phys. Status Solidi C **7**, 1309 (2010).
5) O. Jani, I. Ferguson, C. Honsberg, and S. Kurtz, Appl. Phys. Lett. **91**, 132117 (2007).
6) C. J. Neufeld, N. G. Toledo, S. C. Cruz, M. Iza, S. P. DenBaars, and U. K. Mishra, Appl. Phys. Lett. **93**, 143502 (2008).
7) X. Zheng, R. H. Horng, D. S. Wuu, M. T. Chu, W. Y. Liao, M. H. Wu, R. M. Lin, and Y. C. Lu, Appl. Phys. Lett. **93**, 261108 (2008).
8) J.-K. Sheu, C.-C. Yang, S.-J. Tu, K.-H. Chang, M.-L. Lee, W.-C. Lai, and L.-C. Peng, IEEE Electron Device Lett. **30**, 225 (2009).
9) S. W. Zeng, B. P. Zhang, J. W. Sun, J. F. Cai, C. Chen, and J. Z. Yu, Semicond. Sci. Technol. **24**, 055009 (2009).

10) R.-H. Horng, S.-T. Lin, Y.-L. Tsai, M.-T. Chu, W.-Y. Liao, M.-H. Wu, R.-M. Lin, and Y.-C. Lu, IEEE Electron Device Lett. **30**, 724 (2009).

11) X. M. Cai, S. W. Zeng, and B. P. Zhang, Appl. Phys. Lett. **95**, 173504 (2009).

12) M. J. Jeng, Y. L. Lee, and L. B. Chang, J. Phys. D **42**, 105101 (2009).

13) R. Dahal, B. Pantha, J. Li, J. Y. Lin, and H. X. Jiang, Appl. Phys. Lett. **94**, 063505 (2009).

14) C. L. Tsai, G. S. Liu, G. C. Fan, and Y. S. Lee, Solid-State Electron. **54**, 541 (2010).

15) S.-W. Zeng, X.-M. Cai, and B.-P. Zhang, IEEE J. Quantum Electron. **46**, 783 (2010).

16) J. J. Wierer, A. J. Fischer, and D. D. Koleske, Appl. Phys. Lett. **96**, 051107 (2010).

17) K. Y. Lai, G. J. Lin, Y.-L. Lai, Y. F. Chen, and J. H. He, Appl. Phys. Lett. **96**, 081103 (2010).

18) I. M. Pryce, D. D. Koleske, A. J. Fischer, and H. A. Atwater, Appl. Phys. Lett. **96**, 153501 (2010).

19) B. R. Jampana, A. G. Melton, M. Jamil, N. N. Faleev, R. L. Opila, I. T. Ferguson, and C. B. Honsberg, IEEE Electron Device Lett. **31**, 32 (2010).

20) M. J. Jeng, T. W. Su, Y. L. Lee, Y. H. Chang, L. B. Chang, R. M. Lin, J. H. Jiang, and Y. C. Lu, Jpn. J. Appl. Phys. **49**, 052302 (2010).

21) R.-H. Horng, M.-T. Chu, H.-R. Chen, W.-Y. Liao, M.-H. Wu, K.-F. Chen, and D.-S. Wuu, IEEE Electron Device Lett. **31**, 585 (2010).

22) C. C. Yang, J. K. Sheu, X. W. Liang, M. S. Huang, M. L. Lee, K. H. Chang, S. J. Tu, F. W. Huang, and W. C. Lai, Appl. Phys. Lett. **97**, 021113 (2010).

23) R. Dahal, J. Li, K. Aryal, J. Y. Lin, and H. X. Jiang, Appl. Phys. Lett. **97**, 073115 (2010).

24) J. P. Shim, S. R. Jeon, Y. K. Jeong, and D. S. Lee, IEEE Electron Device Lett. **31**, 1140 (2010).

25) Y. Kuwahara, T. Fujii, Y. Fujiyama, T. Sugiyama, M. Iwaya, T. Takeuchi, S. Kamiyama, I. Akasaki, and H. Amano, Appl. Phys. Express **3**, 111001 (2010).

26) Y. Kuwahara, T. Fujii, T. Sugiyama, D. Iida, Y. Isobe, Y. Fujiyama, Y. Morita, M. Iwaya, T. Takeuchi, S. Kamiyama, I. Akasaki, and H. Amano, Appl. Phys. Express **4**, 021001 (2011).

27) H. C. Lee, Y. K. Su, W. H. Lan, J. C. Lin, K. C. Huang, W. J. Lin, Y. C. Cheng, and Y. H. Yeh, IEEE Photonics Technol. Lett. **23**, 347 (2011).

28) J. R. Lang, C. J. Neufeld, C. A. Hurni, S. C. Cruz, E. Matioli, U. K. Mishra, and J. S. Speck, Appl. Phys. Lett. **98**, 131115 (2011).

29) C.-L. Tsai, G.-C. Fan, and Y.-S. Lee, J. Vac. Sci. Technol. B **29**, 021201 (2011).

30) R. M. Farrell, C. J. Neufeld, S. C. Cruz, J. R. Lang, M. Iza, S. Keller, S. Nakamura, S. P. DenBaars, U. K. Mishra, and J. S. Speck, Appl. Phys. Lett. **98**, 201107 (2011).

31) L. Sang, M. Liao, N. Ikeda, Y. Koide, and M. Sumiya, Appl. Phys. Lett. **99**, 161109 (2011).

32) J. J. Wierer, Jr., D. D. Koleske, and S. R. Lee, Appl. Phys. Lett. **100**, 111119 (2012).

33) S.-B. Choi, J.-P. Shim, D.-M. Kim, H.-I. Jeong, Y.-D. Jho, Y.-H. Song, and D.-E. Lee, Appl. Phys. Lett. **103**, 033901 (2013).

34) S. Valdueza-Felip, A. Mukhtaroba, Q. Pan, G. Altamura, L. Grenet, C. Durand, C. Bougerol, D. Peyrade, F. González-Posada, J. Eymery, and E. Monroy, Jpn. J. Appl. Phys. **52**, 08JH05 (2013).

35) N. G. Young, R. M. Farrell, Y. L. Hu, Y. Terao, M. Iza, S. Keller, S. P. DenBaars, S. Nakamura, and J. S. Speck, Appl. Phys. Lett. **103**, 173903 (2013).

36) Recent researches on InGaN-based solar cells are widely reviewed in A. G. Bhuiyan, K. Sugita, A. Hashimoto, and A. Yamamoto, IEEE J. Photovoltaics **2**, 276 (2012).

37) N. Watanabe, H. Yokoyama, N. Shigekawa, K. Sugita, and A. Yamamoto, Jpn. J. Appl. Phys. **51**, 10ND10 (2012).

38) The band diagrams were simulated using the NEXTNANO3 software package, which can be downloaded from www.nextnano.de.

39) Web [http://rredc.nrel.gov/solar/spectra/].